ESLAB #53: The *Gaia* Universe
Edited by J.H.J. de Bruijne

Long-period variables in the *Gaia* era

Nami Mowlavi[1,2], Michele Trabucchi[3], Thomas Lebzelter[4]

[1] Department of Astronomy, University of Geneva, Ch. des Maillettes 51, 1290 Versoix, Switzerland
[2] Department of Astronomy, Beijing Normal University, 19 XinJieKouWai St., HaiDian District, 100875 Beijing, China
[3] Dipartimento di Fisica e Astronomia Galileo Galilei Università di Padova, Vicolo dell'Osservatorio 3, 35122 Padova, Italy
[4] Department of Astrophysics, University of Vienna, Tuerkenschanzstrasse 17, 1180 Vienna, Austria

arXiv:1907.05359v1 [astro-ph.SR] 11 Jul 2019

Abstract

The second *Gaia* data release (DR2, spring 2018) included a unique all-sky catalogue of large-amplitude long-period variables (LPVs) containing Miras and semi-regular variables. These stars are on the Asymptotic Giant Branch (AGB), and are characterized by high luminosity, changing surface composition, and intense mass loss, that make them of paramount importance for stellar, galactic, and extra-galactic studies.
An initial investigation of LPVs in the Large Magellanic Cloud (LMC) from the DR2 catalog of LPVs has revealed the possibility to disentangle O-rich and C-rich stars using a combination of optical *Gaia* and infrared 2MASS photometry. The so-called *Gaia*-2MASS diagram constructed to achieve this has further been shown to enable the identification of sub-groups of AGB stars among the O-rich and C-rich LPVs.
Here, we extend this initial study of the *Gaia*-2MASS diagram to the Small Magellanic Cloud and the Galaxy, and use a variability amplitude proxy to identify LPVs from the full *Gaia* DR2 archive. We show that the remarkable properties found in the LMC also apply to these other stellar systems. Interesting features, moreover, emerge as a result of the different metallicities between the three stellar environments, which we highlight in this exploratory presentation of *Gaia*'s potential to study stellar populations harboring LPVs.
Finally, we look ahead to the future, and highlight the power of the exploitation of *Gaia* RP spectra for the identification of carbon stars using solely *Gaia* data in forthcoming data releases, as revealed in an *Image of the Week* published by the *Gaia* consortium on the European Space Agency's web site.
These proceedings include three animated images that can be used as outreach material.

1 Introduction

The asymptotic giant branch (AGB) stage is the final evolutionary phase of low- and intermediate-mass stars before becoming white dwarfs. During this phase of high luminosity (they can become brighter than Cepheids), the surface composition is chemically altered by deep convective mixing, and the star loses mass at a high rate (up to 10^{-4} $M_\odot$/yr). Due to these, AGB stars play a key role in stellar and galactic evolution. Furthermore, their light curves show variability on time scales from tens to above a thousand of days, making them classified as long-period variables (LPVs). This, combined with their intrinsic red colors, allows to easily identify them in large-scale surveys. This is specifically true for the *Gaia* all-sky survey, which provides, among other data, G photometry in a main broad optical band, and $G_{\rm BP}$ and $G_{\rm RP}$ photometry in blue and red bands, respectively.

In *Gaia* Data Release 2 (DR2), Mowlavi *et al.* (2018) presented a catalogue of 151'761 LPV candidates with G band variability amplitudes larger than 0.2 mag (amplitudes measured between the 5 and 95% quantiles). Despite the use of selection criteria that aimed at prioritizing low contamination over high completeness – the completeness was estimated to be less than 50% over the entire sky –, this DR2 catalog already doubled the number of known such large-amplitude LPVs at the time of publication. It thereby provided a unique unprecedented catalog for the study of populations of LPVs.

Among the first applications of this catalog, our group investigated the potential of combining the optical *Gaia* $G_{\rm BP}$ and $G_{\rm RP}$ photometry with infrared J and $K_{\rm s}$ photometry from 2MASS. Lebzelter *et al.* (2018) demonstrated on the DR2 LPV candidates of the Large Magellanic Cloud (LMC) that a combination of visual and infrared Wesenheit functions, hereafter called the *Gaia*-2MASS Wesenheit index and denoted ΔW_{G2M}, allows to nicely identify subgroups of AGB stars according to their mass and chemistry. We recall the definition of this index:

$$\Delta W_{G2M} = W_{\rm RP,BP-RP} - W_{\rm K_s,J-K_s} \ , \qquad (1)$$

with

$$W_{\rm RP,BP-RP} = G_{\rm RP} - 1.3\,(G_{\rm BP} - G_{\rm RP}) \qquad (2)$$

$$W_{\rm K_s,J-K_s} = K_s - 0.686\,(J - K_{\rm s}) \qquad (3)$$

In particular, C-rich stars can be distinguished from O-rich stars in the so-called *Gaia*-2MASS diagram, which plots the absolute magnitude (we used $K_{\rm s}$ as it is less sensitive to both interstellar extinction and intrinsic LPV variability than G) versus ΔW_{G2M}. Furthermore, low-mass, intermediate-mass and massive O-rich AGB stars, as well as supergiants, populate distinct regions in this diagram, enabling to identify them in a population of LPVs with known distances. This provides new opportunities for stellar populations studies (e.g. age, chemical composition) from the study of subpopulations of LPVs harbored therein. The reader is referred to Lebzelter *et al.* (2018) for a presentation of the properties and potential usage of this new *Gaia*-2MASS diagram.

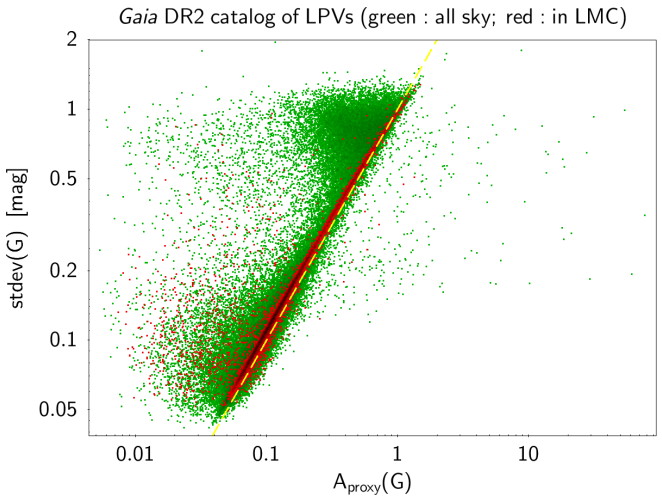


Figure 1: Variability amplitude proxy (x abscissa) versus standard deviation of the G magnitude time series (y ordinate) for all *Gaia* DR2 LPV candidates (in green). The subset of candidates belonging to the LMC are shown in red. The yellow dashed line is a $y=x$ diagonal line to guide the eyes.

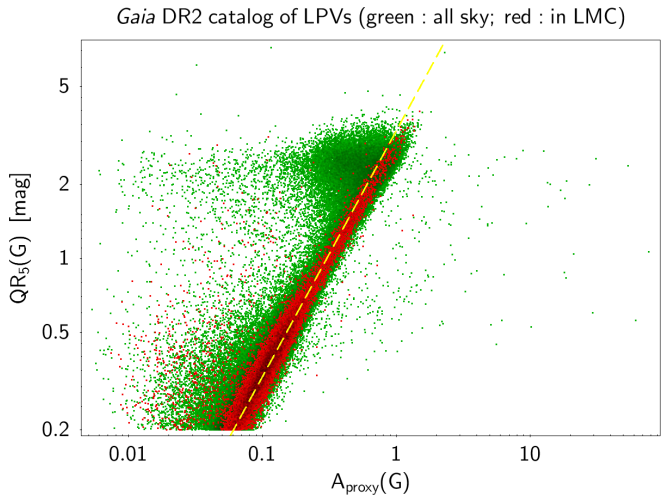


Figure 2: Same as Fig. 1, but with the variability amplitude proxy plotted versus the 5-95% quantile range of the G magnitude time series. The yellow dashed line is $y=3.3*x$.

This ESLAB #53 conference aimed at showing the unique advances made possible by *Gaia* DR2 in various fields of astrophysics. In this spirit, we show in these proceedings the potential of *Gaia* to study populations of LPVs using the approach introduced in Lebzelter *et al.* (2018), but extended to the entire DR2 catalog (the study in Lebzelter *et al.* (2018) was based on the restricted list of candidates published in the DR2 catalog of LPVs) and to various stellar environments (the study in Lebzelter *et al.* (2018) was limited to the LMC). To achieve this, we first need to be able to identify LPVs in the entire DR2 archive. This is addressed in Sect. 2, and applied to the LMC in Sect. 3. Populations of LPVs in the Small Magellanic Cloud (SMC) and in the Galaxy are then explored using this technique in Sects. 4 and 5, respectively.

Given the paramount importance of the question of C-rich star identification for the chemical return of AGB stars and for the chemical evolution of the Galaxy (and of galaxies in general), we devote Sect. 6 to a brief presentation of the unique potential of *Gaia* in this respect. We already showed in Lebzelter *et al.* (2018) the possibility of this identification using the *Gaia*-2MASS diagram, as recalled above. Its application to the SMC and the Galaxy, in addition to the LMC, is discussed in Sect. 6.1. Yet, the potential of *Gaia* in its future data releases is expected to be even greater, with the provision of information extracted from the epoch RP spectra of the *Gaia* red spectro-photometer. This was shown in the *Gaia Image of the Week* (IoW) of 15/11/2018 published on the *Gaia* web pages of the European Space Agency (ESA)[1], and is recalled in Sect. 6.2. Section 7 finally ends these proceedings with some conclusions.

For illustration and outreach purposes, movies/animated images of Fig. 12 (*Gaia*-2MASS diagram), of Fig. 13 (photometric and spectroscopic variability of an O-rich AGB star), and of Fig. 14 (idem, but of a C-rich AGB star) are made available at `https://zenodo.org/record/3237087`.

[1] `https://www.cosmos.esa.int/web/gaia/iow_20181115`

2 The sample of LPV candidates

Similarly to the sample selection done in the *Gaia* DR2 catalog of LPVs, we aim here at identifying *Gaia* red giants with variability amplitudes larger than 0.2 mag in G. The variability amplitude proxy used to achieve this is described in Sect. 2.1, and the procedure to select large-amplitude LPV candidates from the full *Gaia* archive is presented in Sect. 2.2.

2.1 Variability amplitude proxy

In the DR2 catalog of LPVs (Mowlavi *et al.*, 2018), the variability amplitude is provided through either the standard deviation or the 5-95% quantile range $QR_5(G)$ of their G magnitude time series. These quantities are not available in the *Gaia* DR2 archive for sources that have no variability-specific information in the archive. They cannot be computed either, since the light curves of these sources are not published in DR2.

We can, however, use the uncertainty $\varepsilon(\bar{F}(G))$ of the mean G flux $\bar{F}(G)$ published for each source, which contains information on both the uncertainties of the individual measurements due to noise and on the intrinsic scatter of the flux time series due to stellar variability (see Sect. 5.3.5 of the *Gaia* DR2 documentation in Busso *et al.*, 2018). Since the intrinsic scatter of large-amplitude LPVs is much larger (≥ 0.2 mag) than the typical level of photometric uncertainties at the magnitudes considered for LPVs (few milli-magnitude uncertainties at $G \lesssim 16$ mag), the noise of the measurements has a negligible contribution to $\varepsilon(\bar{F}(G))$ for these stars. The quantity $A_{\rm proxy}(G)$ defined by

$$A_{\rm proxy}(G) = \sqrt{N_{\rm obs}}\, \varepsilon(\bar{F}(G))/\bar{F}(G)\ , \qquad (4)$$

where $N_{\rm obs}$ is the number of (per-CCD) observations, is then a useful proxy for the variability amplitude of stellar origin for large-amplitude LPVs. All quantities in Eq. 4 are available in DR2. This approach was already used by Deason *et al.* (2017) to identify Mira variables in *Gaia* DR1.

In these proceedings, we will call the variability amplitude proxy given by Eq. 4 simply as the 'variability proxy'.

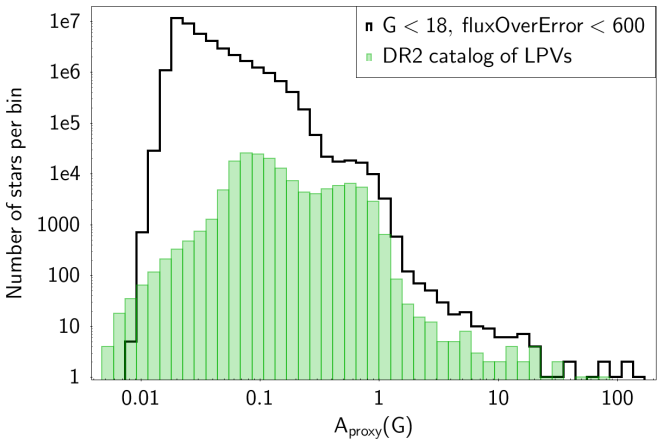


Figure 3: Black histogram: Distribution of the variability amplitude proxy of all sources in the *Gaia* DR2 archive that are brighter than $G = 18$ mag and that have mean G flux over error ratios $\bar{F}(G)/\varepsilon(\bar{F}(G)) < 600$. Green histogram: Same as the black histogram, but for the sources published in the specific DR2 catalog of LPVs.

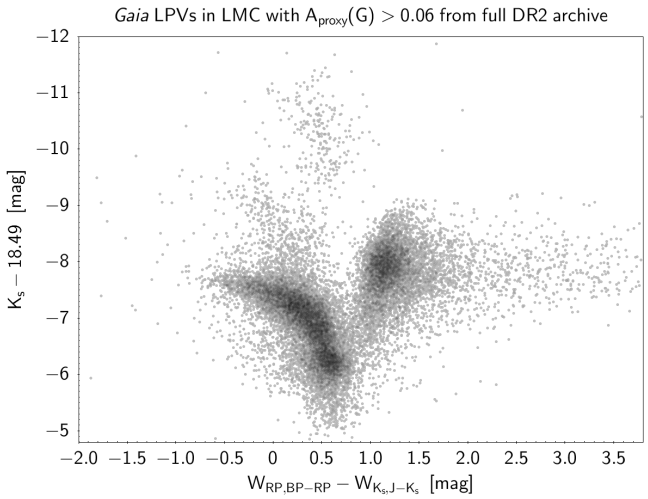


Figure 4: *Gaia*-2MASS diagram of large-amplitude LPV candidates in the LMC selected from the full *Gaia* DR2 archive (see text) with the condition $A_{proxy} > 0.06$ for the variability proxy and having 2MASS cross matches with $J < 14.5$ mag and $K_s < 14.5$ mag.

The relation between $A_{\rm proxy}(G)$ and the standard deviation of the G magnitude time series of large-amplitude LPVs can be checked on the sources published in the DR2 catalog of LPVs, for which the standard deviations are available. The result is shown in Fig. 1. An almost one-to-one relation is obtained, as expected, except for a subset of sources which have a value of their (flux-based) variability proxy smaller than their (magnitude-based) standard deviation (only very few sources have their variability proxy larger than their magnitude-based standard deviation).

The relation between the variability proxy and the 5-95% quantile range $QR_5(G)$ used in DR2 to characterize the variability amplitudes of LPVs is shown in Fig. 2. The majority of sources are close to the linear relation $QR_5(G) = 3.3{*}A_{\rm proxy}(G)$. Sources that deviate from the linear relation have a far-from-optimal sampling of measurements. For the majority of these sources, the standard deviation (and hence the variability proxy) underestimates the variability range. For example, for sources in the LMC shown in red in Fig. 2, the standard deviation of sources close to the South Ecliptic Pole will have too small standard deviations due to the large number of measurements acquired during the first month of the mission[2] compared to the standard deviations they would have if they had a regular sampling over their (much longer than one month) pulsation cycles.

Typical values of the variability proxy expected for LPVs can be derived from Fig. 2. Miras, which pulsate in the fundamental mode, were shown in Mowlavi *et al.* (2018) to have $QR_5(G) \gtrsim 1$ mag. This translates to $A_{\rm proxy}(G) \gtrsim 0.3$. Long-period variables with $QR_5(G) \lesssim 1$ mag, on the other hand, mainly consist of semi-regular variables (SRVs), pulsating in overtone modes. They will have $A_{\rm proxy}(G) \lesssim 0.3$.

[2]A specific scanning law, the Ecliptic Pole Scanning Law (EPSL), was used during the one-month *Gaia* commissioning phase, whereby sources at the ecliptic poles were observed every six hours (spacecraft rotation period) in each of the two *Gaia* fields of view.

2.2 The data

The variability proxy is not an indexed column in the *Gaia* archive, and thus cannot be used to select samples based on $A_{\rm proxy}(G)$. We therefore used the ratio $\bar{F}(G)/\varepsilon(\bar{F}(G))$, which is indexed in the archive, and downloaded all sources with $\bar{F}(G)/\varepsilon(\bar{F}(G)) < 600$ ($\rightarrow$ 41'508'986 sources). A comparison of the variability proxy distribution in this sample with the variability proxy distribution in the sample of DR2 catalog of LPVs, shown in Fig. 3, reveals that the criterion allows to retrieve the great majority (98.6%) of the sources present in the latter catalog. We are therefore confident that the majority of sources from the full *Gaia* archive with $QR_5(G) > 0.2$ are present in the downloaded sample.

We then selected as large-amplitude LPVs all red sources ($G_{\rm BP} - G_{\rm RP} > 1.5$ mag, $\rightarrow$ 19'205'377 sources) that have $A_{\rm proxy}(G) > 0.06$ mag ($\rightarrow$ 2'952'438 sources). This limit on the variability proxy was chosen to comply (see Fig. 2) with the amplitude condition $QR_5(G) > 0.2$ mag used in the DR2 catalog of LPVs . Finally, we restricted the sample to sources that have 2MASS crossmatches with $J < 14.5$ mag and $K_s < 14.5$ mag ($\rightarrow$ 1'379'652 sources). These conditions on the 2MASS photometry are intended to provide near-infrared data with good quality to construct *Gaia*-2MASS diagrams.

This final set of 1'379'652 large-amplitude LPV candidates is used in the next sections to extract samples in the LMC, the SMC and the Galaxy.

criteria	LMC sample	SMC sample
RA	50° to 105°	0° to 35°
DEC	−77° to −61°	−80° to −65°
PM(RA)	1.2 to 2.5 mas/yr	−0.3 to 1.6 mas/yr
PM(DEC)	−0.8 to 1.5 mas/yr	−1.9 to −0.7 mas/yr
ϖ	< 0.5 arcsec	< 0.5 arcsec

Table 1: Selection criteria for stars in the LMC and SMC.

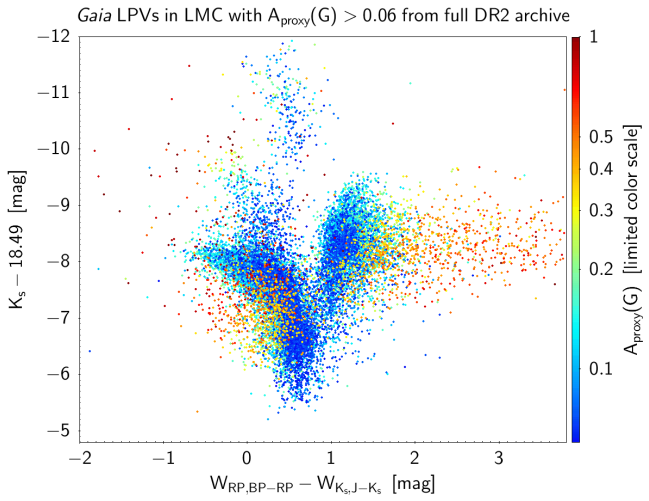


Figure 5: Same as Fig. 4, but color-coded with the variability amplitude proxy of each source according to the color scale shown on the right of the figure. Sources with $A_{\rm proxy}(G) < 0.06$ or $A_{\rm proxy}(G) > 1$ are plotted with the color at the respective end of the color scale. The subset of sources with $A_{\rm proxy}(G) > 0.3$ has been plotted on top of the subset with $A_{\rm proxy}(G) < 0.3$ for visibility purposes, to ensure that the former ones are all shown on top of the latter ones.

3 LPVs in the Large Magellanic Cloud

Members of the LMC are selected on the basis of their locations in the sky, their proper motions, and their parallaxes. The selection criteria are the same as the ones used in Lebzelter *et al.* (2018), recalled in Table 1. With the conditions mentioned in Sect. 2.2 on *Gaia* color, variability proxy and 2MASS photometry, the sample of LPVs in the LMC amounts to 20'486 sources. This is almost twice the number of sources (10'989 sources) of the LMC published in the *Gaia* DR2 catalog of LPV candidates.

The distribution in the *Gaia*-2MASS diagram of these LMC LPV candidates is shown in Fig. 4. The various branches related to different stellar mass regimes identified by Lebzelter *et al.* (2018) are clearly visible for this larger sample as well.

Figure 5 shows the same diagram as in Fig. 4, but with each point color-coded according to the value of $A_{\rm proxy}(G)$ of the star. Mira candidates are plotted on top of the other stars to make them all visible. Their distribution in the diagram seems to follow a slightly different pattern than the smaller amplitude SRVs, with Miras spreading more over the diagram than SRVs. This is more clearly shown in Fig. 6, which separates the two groups of stars, Mira candidates and SRV candidates, in the top and bottom panels, respectively. The discussion on this feature must distinguish the case of C-rich stars (right half of the diagram at $\Delta W_{G2M} \gtrsim 0.8$ mag) from the case of O-rich stars (left half of the diagram).

The C-rich Miras in Fig. 6 (bottom panel) extend towards very large ΔW_{G2M} values compared to the SRVs (top panel). In Lebzelter *et al.* (2018), we named these stars 'extreme C-stars', and we suggested that these are high-mass-loss objects. The fact that only large-amplitude variables are found here confirms the widely accepted connection between large-amplitude variability and mass-loss (e.g. Höfner & Olofsson, 2018).

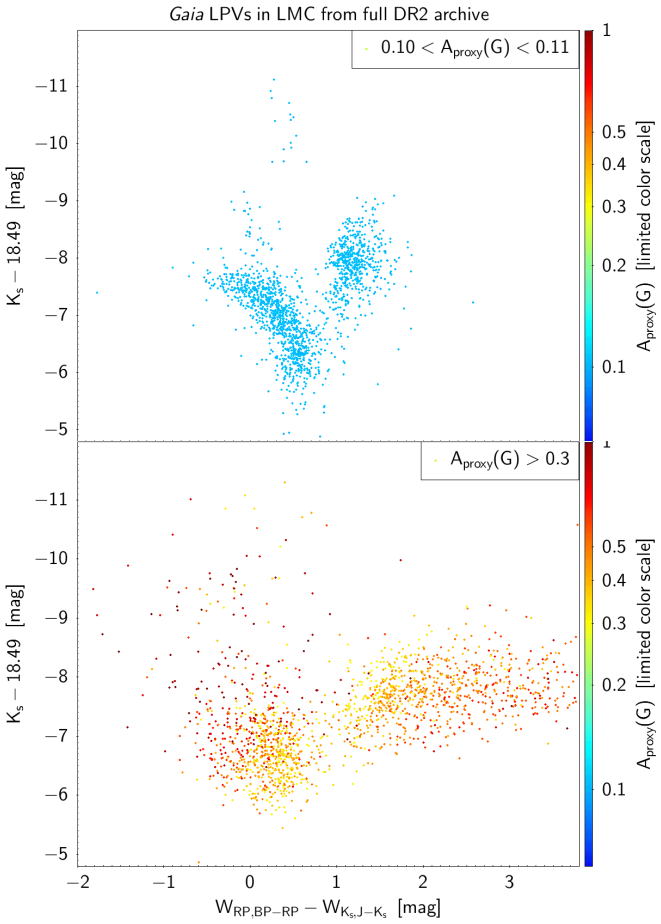


Figure 6: Same as Fig. 5, but for samples of red giants within restricted ranges of the variability proxy. The top panel is restricted to $0.10 < A_{\rm proxy}(G) < 0.11$ (containing mainly semi-regular variables), while the bottom panel covers $A_{\rm proxy}(G) > 0.3$ (containing predominantly Miras).

Concerning O-rich Miras, many of them are found below the lowest-luminosity branch in Fig. 5 (branch (a) in Lebzelter *et al.*, 2018). A detailed analysis of this group is beyond the scope of these proceedings. However, we note that circumstellar reddening resulting from heavy mass loss (see, e.g., McDonald *et al.*, 2018) and the appearance of significant amounts of water absorption in the near-infrared spectra (see Fig. 2 in Aringer *et al.*, 2002) are expected to reduce the $K_{\rm s}$-band brightness of these stars. Furthermore, the $K_{\rm s}$-band magnitudes used here are single-epoch observations, leading to a larger scatter in $K_{\rm s}$ for large-amplitude stars. These effects affect less SRVs because they have, on average, less circumstellar reddening and because their amplitude of variability is smaller than for Miras. These effects also lead to a spread of the ΔW_{G2M} values of Miras, but to a lesser degree because the Wesenheit index partly corrects for the reddening effect. In summary, the $K_{\rm s}$ magnitudes of O-rich Miras are expected to be, on the mean, larger (fainter) than those of O-rich SRVs, and to display a larger spread due to both the larger intrinsic variability amplitudes of Miras and the single-epoch nature of the 2MASS survey.

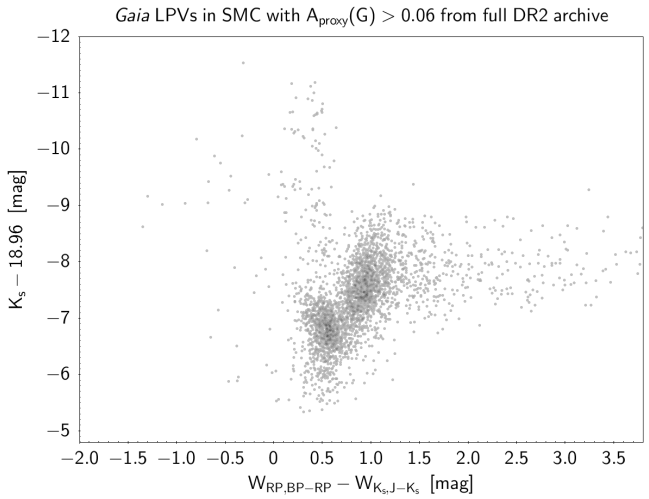


Figure 7: Same as Fig. 4, but for the SMC.

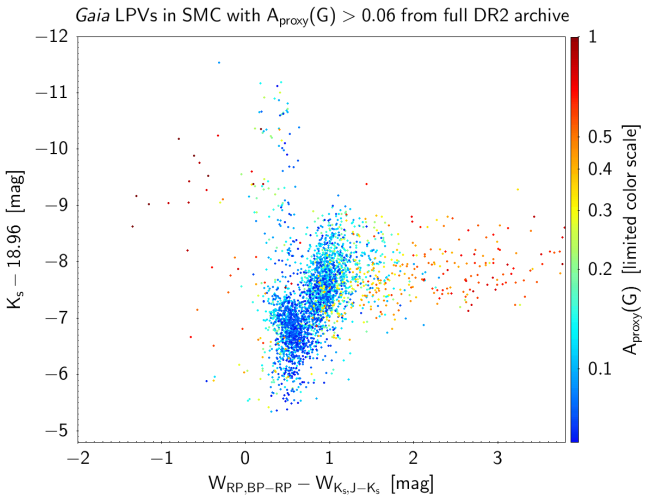


Figure 8: Same as Fig. 5, but for the SMC.

4 LPVs in the Small Magellanic Cloud

The selection criteria for members of the SMC are given in Table 1. With the conditions on *Gaia* color, variability proxy, and 2MASS photometry mentioned in Sect. 2.2 to select large-amplitude LPV candidates, we reach a sample of 3'208 sources.

The *Gaia*-2MASS diagram for the SMC is shown in Figs. 7 and 8. There are two main differences compared to the equivalent diagrams for the LMC (Figs. 4 and 5, respectively). First is the larger proportion of C-rich relative to O-rich stars in the SMC than in the LMC. This is a well known fact, due to the lower metallicity of the SMC. Indeed, at low metallicity, AGB stars experience more easily the third dredge-up process that mixes carbon from the deep interior where it is synthesized to the surface, and at an earlier stage on their AGB phase. In addition, the oxygen abundance is lower in the atmosphere of an AGB star in the SMC than in the LMC, such that a smaller number of dredge-up events is needed to reach C/O>1. As a result, the star spends an increased fraction of its lifetime as a C star (see, e.g., Fig. 22 in Marigo & Girardi, 2007). Similar conclusions are drawn in the literature from, for example, the observation of stellar clusters in the SMC (Frogel *et al.*, 1990) and the analysis of the period-luminosity diagram of LPVs in the SMC (Soszyński *et al.*, 2011).

The second striking feature in Fig. 7 is the truncation of the O-rich low-mass branch towards low ΔW_{G2M} values compared to the *Gaia*-2MASS diagram of the LMC (Fig. 4): there is practically no LPV with $\Delta W_{G2M} < 0.2$ mag in the SMC. This may be a direct consequence of the increased third dredge-up efficiency with decreasing metallicity, the O-rich star becoming C-rich before reaching the far left side of the *Gaia*-2MASS diagram.

Let us, however, remark that the specific star formation history of the SMC, a subtle interplay between metallicity and evolution, the larger surface temperatures usually characterizing lower metallicity stars, and/or the smaller Ti abundance due to lower metallicity, all could play a role in shaping the distribution of O-rich LPVs in the *Gaia*-2MASS diagram. We further note from Fig. 8 that almost all O-rich stars beyond the truncation limit of branch (a) on the left of the diagram, with $\Delta W_{G2M} < 0.2$ mag, are Miras.

5 LPVs in the Galaxy

The study of LPVs in the Galaxy is much more challenging than in the Magellanic Clouds. First, because they cannot be assumed to lie at a given known distance as is the case for the LMC and the SMC. Here *Gaia* will be of key help by providing parallax measurements. Second, because Galactic sources are affected by differential interstellar reddening that varies greatly depending on sky position and distance into the Galaxy.

We consider two samples of Galactic LPVs, selected on their relative parallax uncertainties (in addition to the LPV criteria on color, variability amplitude and 2MASS photometry precision described in Sect. 2.2). The first sample is restricted to all LPV candidates with relative *Gaia* DR2 parallax uncertainties better than 10%, while the second sample contains a larger set with parallax uncertainties up to 15%. In both samples, we have to exclude potential Young Stellar Objects that can be contaminants to LPVs (see Mowlavi *et al.*, 2018). We do this by imposing an upper limit on the absolute(G) magnitude of LPVs, that depends on the $G_{\rm BP}$-$G_{\rm RP}$ color as defined by the dashed line in Fig. 28 of Mowlavi *et al.* (2018), i.e. absolute$(G) < -2.6 + 1.72 * (G_{\rm BP} - G_{\rm RP})$. The resulting samples contain respectively 4803 and 12'820 LPV candidates.

The *Gaia*-2MASS diagrams of these two samples of Galactic large-amplitude LPV candidates are shown in Figs. 9 and 10, respectively. We note the following points:

- There are much less C-rich relative to O-rich stars in the Galaxy than in the Clouds (compare Fig. 9 with Figs. 4 and 7). This agrees with the decrease of third dredge-up efficiency with increasing metallicity, combined with the larger O abundances in the envelope of AGB stars, as already noticed in Sect. 4 when comparing the representative diagrams of the SMC and LMC.

- The distribution of O-rich LPVs in branch (a) of the diagram (containing low-mass AGB stars as well as stars at the tip of the red giant branch) covers, at any given absolute $K_{\rm s}$ magnitude, a much wider range of ΔW_{G2M} in the Galaxy than in the Clouds. In Sect. 4, we noticed a

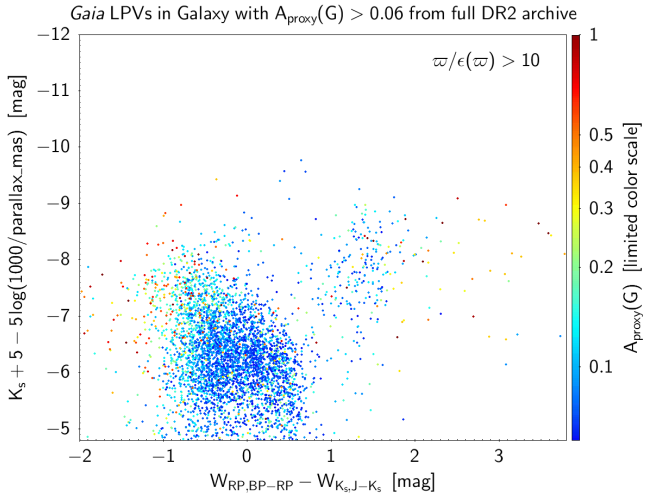


Figure 9: Same as Fig. 5, but for Galactic LPVs with relative DR2 parallax uncertainties better than 10%.

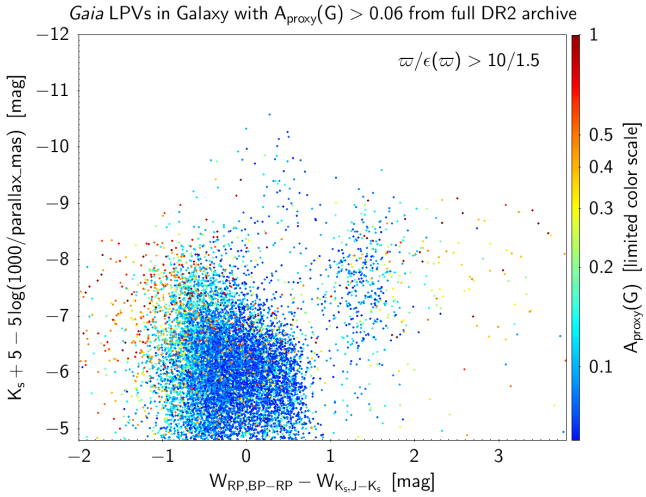


Figure 10: Same as Fig. 5, but for Galactic LPVs with relative DR2 parallax uncertainties better than 15%.

truncated extension of branch (a) in the SMC compared to the LMC. Extrapolating this observed difference between the SMC and LMC to the larger metallicities (on the mean) of the Galaxy would agree with the smaller (i.e. larger negative) values of ΔW_{G2M} observed in the sample of Galactic LPVs (compare Fig. 9 with Figs. 4 and 7). Interstellar (and possibly circumstellar) reddening would then explain the distribution of branch (a) in Figs. 9 and 10 towards the faint (lower) side of the diagram. The wide distribution of branch (a) in both axes in these figures would thus result from the combined effect of O-rich AGB stars turning much later into C-rich stars in the Galaxy, if at all, and extinction (plus possibly other effects as discussed in Sect. 4). But see also the note at the end of this section on parallax determinations.

- Despite the previous point, the group of C-rich stars still stands distinct from the group of O-rich stars in the *Gaia*-2MASS diagram (Figs. 9 and 10). This remarkable property of the *Gaia*-2MASS diagram results from the fact that reddening leads to a slight displacement of the representing point in the diagram *away* from the vertical line separating the two groups of stars: a reddened C-rich star will be displaced to larger ΔW_{G2M} values, while reddened O-rich stars will be displaced to smaller (negative) values of this index.

- Only very few massive AGB and red supergiants are present in the Galactic samples of the extended Solar neighborhood considered here.

Let us finally issue a warning on the parallaxes. Attention must be paid that systematics and biases may exist in the DR2 parallax determinations of red giants. A bias towards the exclusion of the reddest giants in a parallax-precision-limited sample was already stressed in Mowlavi *et al.* (2018) (see in particular their Fig. 24), due to their fainter magnitudes (maximum of spectrum emission displaced to longer wavelengths in the infrared). In addition, there were limitations in DR2 parallaxes (Lindegren *et al.*, 2018).

6 Carbon star identification

The identification of C-rich and O-rich stars using *Gaia* and 2MASS data is addressed in Sect. 6.1, with a particular focus on the effect of metallicity. The potential of achieving the distinction in future *Gaia* data releases using only *Gaia* data is then highlighted in Sect. 6.2.

6.1 In the *Gaia*-2MASS diagram

With *Gaia* DR2, Lebzelter *et al.* (2018) showed how the combination of optical and infrared data allows to distinguish between O-rich and C-rich stars in the *Gaia*-2MASS diagram, where these two types of LPVs occupy distinct regions. It was shown that this optical+infrared diagram is more powerful than the infrared color-magnitude diagram usually used in the literature for this purpose. The improvement is illustrated in Fig. 12, of which an animated image is available (see caption of the figure).

With the samples of LPV candidates presented in these proceedings for the SMC, LMC and Galaxy, we can investigate the metallicity dependence of the delineation between C-rich and O-rich LPVs in the *Gaia*-2MASS diagram. For this purpose, the histograms of ΔW_{G2M} are shown in Fig. 11 for the three samples. The value of ΔW_{G2M} at the minimum of the histograms approximately delineates the border between O-rich (values smaller than this limit) and C-rich (values larger than this limit) stars. The exact value actually depends on the absolute K_s magnitude, the border not being a straight vertical line in the *Gaia*-2MASS diagram, as seen in Fig. 1 of Lebzelter *et al.* (2018). The histograms of the different stellar samples nevertheless suggest a slight metallicity dependence of the borders separating the different subgroups of AGB stars, this border shifting to slightly larger values of ΔW_{G2M} with an increase of the (mean) metallicity of the considered stellar sample. Further studies, outside the scope of these proceedings, should be performed on the 2-dimension distribution of sources in the *Gaia*-2MASS diagram, and distinguishing various stellar populations in the Galaxy (halo, thin/thick disk, bulge), in order to reach a full understanding of the metallicity dependence of the boarders between the different regions in this diagram.

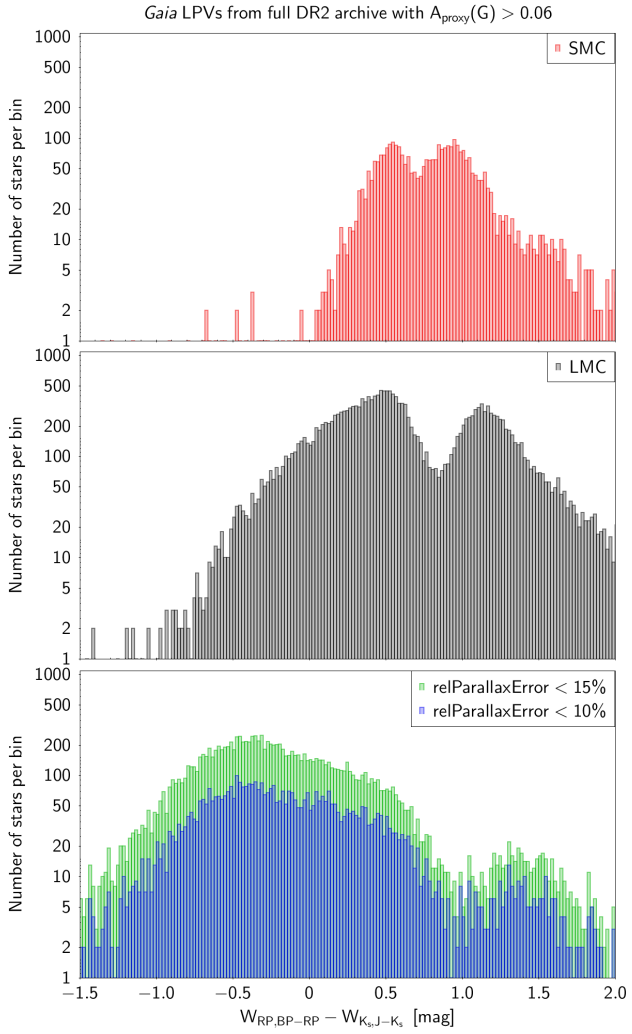


Figure 11: Histograms of the *Gaia*-2MASS Wesenheit index ΔW_{G2M} of large-amplitude LPV candidates selected with $A_{\rm proxy}(G) > 0.06$ from the full *Gaia* DR2 archive. Top panel: candidates in the SMC; middle panel: in the LMC; bottom panel: in the Galaxy with relative parallax uncertainty better than 10% in blue and better than 15% in green.

6.2 Using solely *Gaia* data

With the *Gaia* IoW of 15/11/2018 published on ESA's web pages[1], the *Gaia* Consortium revealed the potential of identifying C stars in the next *Gaia* data releases[3] using only *Gaia* data, i.e. without the necessity of infrared information. The IoW showed that the red spectro-photometer (RP) on board of *Gaia* provides low-resolution spectra that are adequate for a discrimination between O-rich and C-rich stars, from the signature of molecular bands specific to either O-rich (mainly TiO and VO) or C-rich (mainly C_2, CH, and CN) cool stellar atmospheres. The reader is referred to the explanations provided therein for more information.

[3] *Gaia* RP spectra are not planned to be released in DR3 (see *Gaia* data release scenario at `https://www.cosmos.esa.int/web/gaia/release`), but the *Gaia* Consortium aims to provide C-rich and O-rich star identification for LPVs.

The IoW also showed that the large stellar surface temperature variations of Miras over their pulsation cycles can lead to significant variations in the shapes of the spectra as a function of pulsation phase. With *Gaia*, this can be effectively handled based on the multiple epoch spectra taken for each observed source. The IoW illustrated this power with the RP epoch spectra recorded over the DR2 period for two Miras, the O-rich Mira T Aqr (pulsation period $P = 203$ d) and the C-rich Mira RU Vir ($P = 425$ d). The links between these RP spectral variations and the photometric variability are shown in Figs. 13 and 14 for T Aqr and RU Vir, respectively. Animated versions of the figures are available on the web as mentioned in the caption of Fig. 13 .

7 Conclusions

Lebzelter *et al.* (2018) have shown the power of combining optical *Gaia* and infrared 2MASS data to identify sub-groups of AGB stars among LPVs, including the distinction between C-rich and O-rich stars. The main tool was the *Gaia*-2MASS diagram shown in Fig. 4. They based their study on the LMC LPVs published in the *Gaia* DR2 catalog of LPVs (Mowlavi *et al.*, 2018).

In these proceedings, we first showed how the study can be extended to the set of LPVs from the whole *Gaia* DR2 archive using a variability amplitude proxy based on the published uncertainties of the mean G fluxes. We then explored the *Gaia*-2MASS diagram for *a)* the set of LPVs in the LMC extracted from the full *Gaia* DR2 archive, *b)* the SMC, and *c)* the Galaxy.

In the LMC, the *Gaia*-2MASS diagram of the extended set of LPVs confirms the properties set forth in Lebzelter *et al.* (2018). In addition, it is shown (see Fig. 6) that the extreme C-rich branch is almost exclusively populated by Miras, and that O-rich Miras display a spread in the diagram due to both physical properties and observational biases (see Sect. 3).

In the SMC, the *Gaia*-2MASS diagram displays striking differences compared to the LMC, attributed to the lower metallicity of the SMC (see Sect. 4).

The study in the Galaxy is more challenging than in the Clouds due to the differential reddening affecting Galactic sources. The analysis of the *Gaia*-2MASS diagram has nevertheless led to interesting conclusions, one of them being that the clear distinction between O-rich and C-rich stars remains valid even in the presence of reddening (see Sect. 5).

Finally, we showed in Sect. 6.1 that the boundary separating O-rich and C-rich LPVs in the *Gaia*-2MASS diagram depends slightly on metallicity. We then ended in Sect. 6.2 with the interesting prospect revealed in the *Gaia* IoW of 15/11/2018 that C-rich and O-rich AGB stars can be identified using *Gaia* RP spectra, thereby removing the need to rely on infrared data. This would allow to have a homogeneous set of C-rich AGB star candidates based solely on *Gaia* data in forthcoming *Gaia* data releases. The IoW also showed the essential variability of the spectral features of Miras, especially of O-rich Miras. To illustrate this, we produced animated images (Figs. 13 and 14) of the simultaneous photometric and RP spectroscopic variations of the two Miras shown in the IoW, that are adequate for public outreach.

Acknowledgments

We would like to thank the whole *Gaia* consortium for the immense work performed in the processing and analysis of

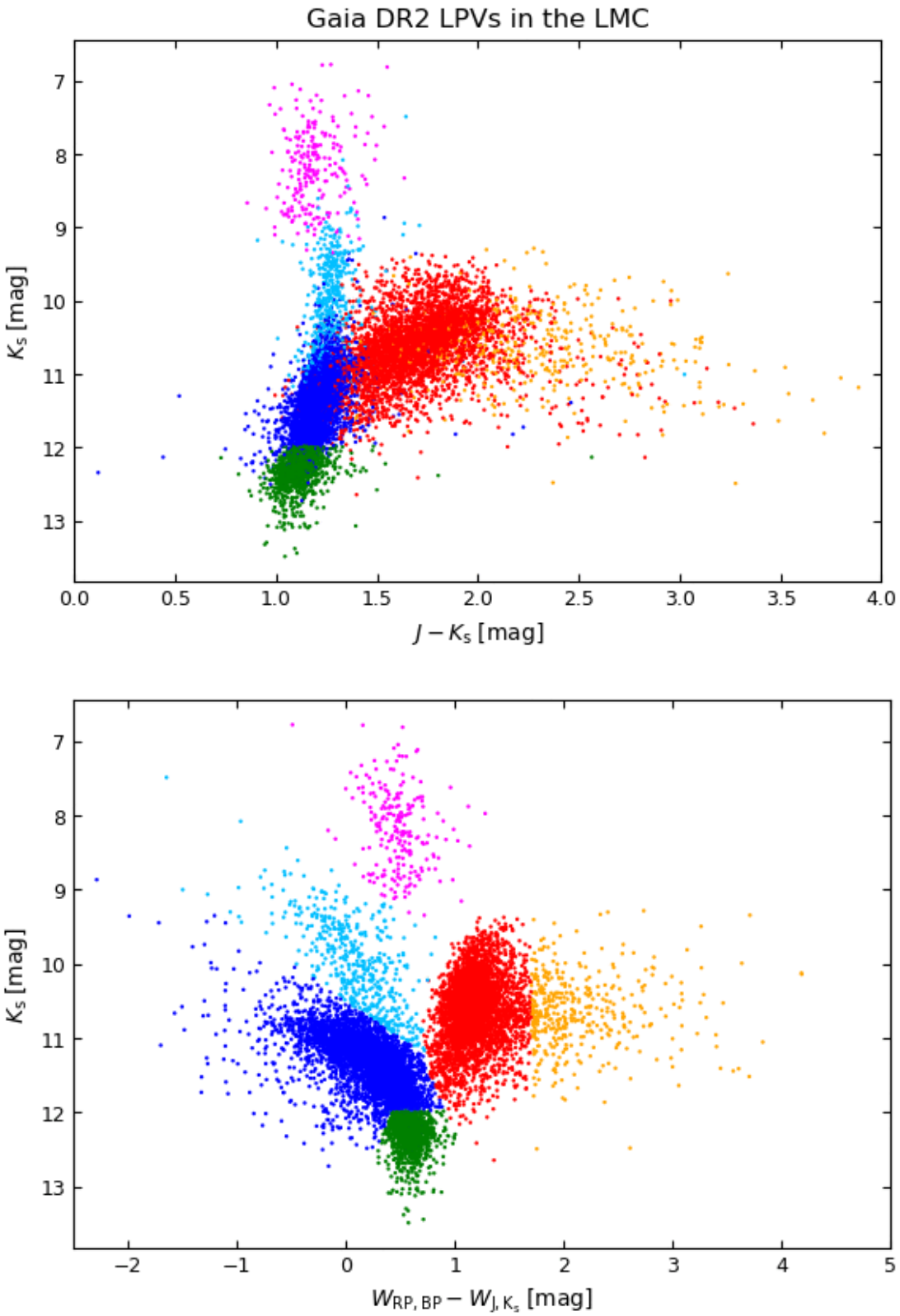


Figure 12: Distribution of the LMC LPV candidates from the *Gaia* DR2 catalog of LPVs (Mowlavi *et al.*, 2018) in the 2MASS color-magnitude diagram (top panel, units of both axes in magnitude) compared to their distribution in the *Gaia*-2MASS diagram (bottom panel). The colors indicate the different subgroups of AGB stars identified in Lebzelter *et al.* (2018).
An animated image illustrating the shift from the top to bottom diagrams is available in the Zenodo archive at `https://zenodo.org/record/3237087`.

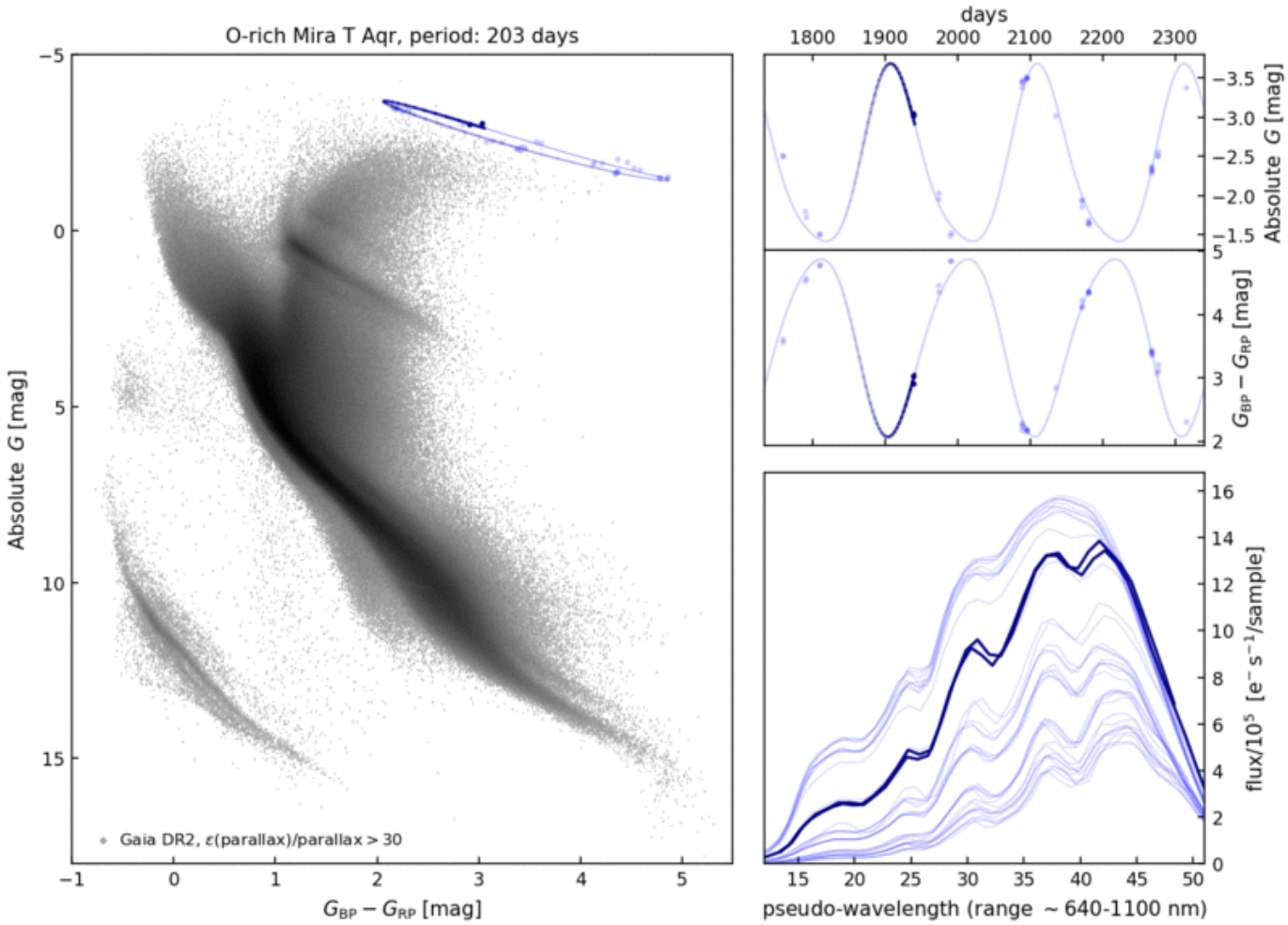


Figure 13: Photometric and spectroscopic variability of the O-rich Mira T Aqr ($P = 203$ d) during the 22 months of data covered by *Gaia* DR2. **Left panel:** Photometric variability of the star (in blue) in the *Gaia* color – Absolute G magnitude diagram. The background stars are the set of *Gaia* DR2 sources brighter than $G = 18$ with parallax over parallax error ratios $\varpi/\varepsilon(\varpi) > 30$ and good BP+RP excess factors. **Right top panel:** Time series of the G magnitude and $G_{\rm BP}$-$G_{\rm RP}$ color of the star, from the *Gaia* DR2 archive. The blue lines are Fourier series fits to the *Gaia* DR2 measurements (shown as blue filled circles) in each of the two time series. The blue line in the left panel results from these fits. **Right bottom panel:** Epoch RP spectra of the star from the *Gaia* IoW of 15/11/2018 (the credits are the same as in the IoW, see `https://www.cosmos.esa.int/web/gaia/iow_20181115`). The X-axis is a pseudo-wavelength covering the approximate range from 640 to 1100 nm. The dark blue points/spectra identify the same times in all panels.
An animated version of the figure is available in the Zenodo archive at `https://zenodo.org/record/3237087`.

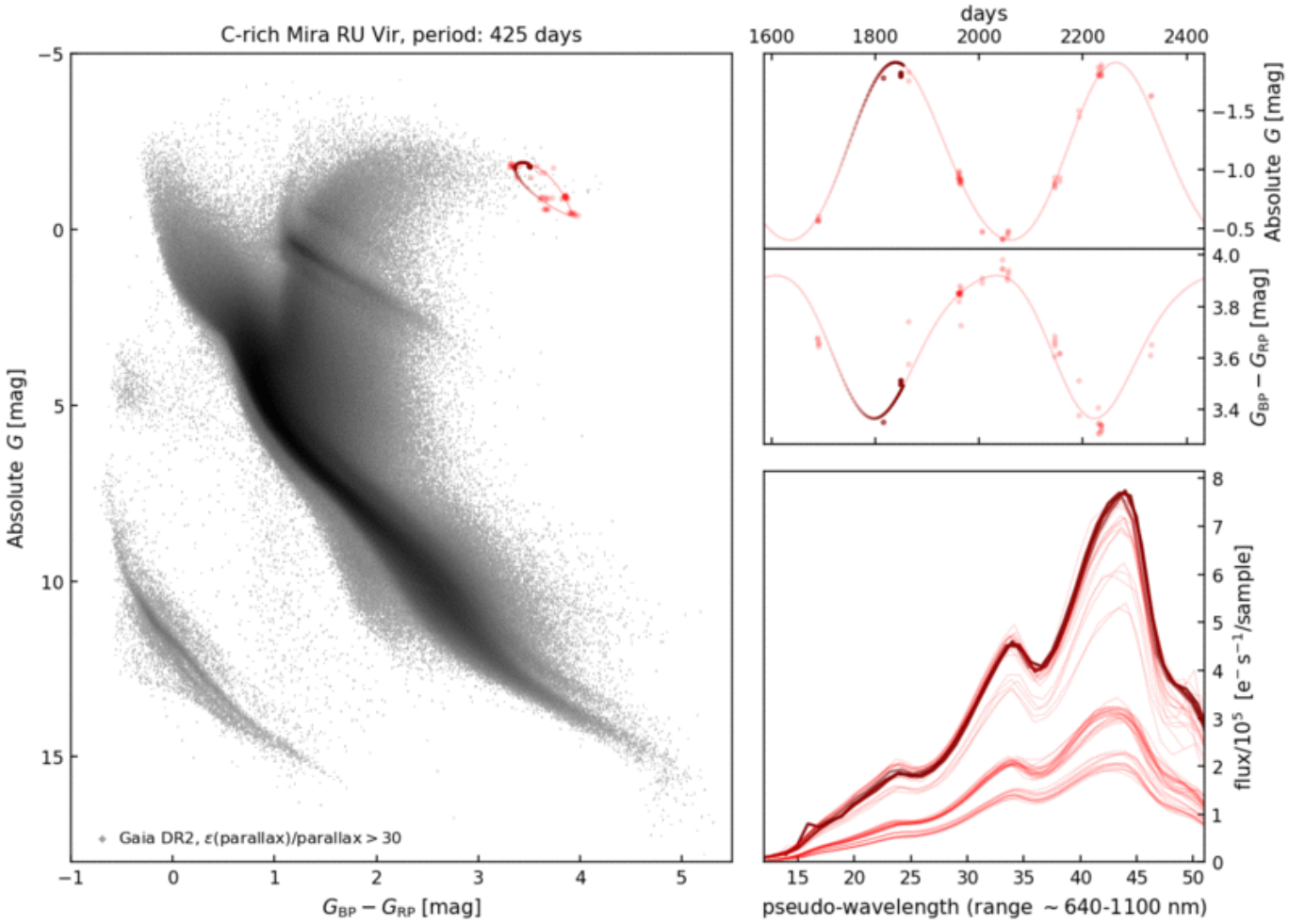


Figure 14: Same as Fig. 13, but for the C-rich Mira RU Vir ($P = 425$ d). The blue color of Fig. 13 has been replaced by red color in all panels.

the *Gaia* data and their successive releases to the scientific community. Two of us (NM and TL) are part of the *Gaia* Data Processing and Analysis Consortium (DPAC), and responsible therein for the analysis and publication of LPVs within Coordination Unit 7 (CU7). In this respect, we would like to take this opportunity to thank more specifically *a)* the CU5 team in Cambridge responsible for the photometry and spectroscopy, *b)* the CU7 and Data Processing Center teams in Geneva responsible for the processing of variable objects, and *c)* in particular our colleague Isabelle Lecoeur-Taïbi therein who actively contributes with us in the processing and analysis of LPVs. Credits for the epoch RP spectra shown in these proceedings are the same as in the ESA/*Gaia* IoW of 15/11/2018[1], from where they were taken, and we thank the permission to reproduce them here. We further thank Maria Süveges for her help in the preparation of these spectra data for the production, by one of us (MT), of the movies and animated images accompanying Figs. 13 and 14. Finally, thanks go to Walter Nowotny for additional model computations performed to investigate the effects of reddening on the properties in the *Gaia*-2MASS diagram. MT acknowledges the support from the ERC Consolidator Grant funding scheme (*project STARKEY*, G.A. n. 615604).
This work has made use of data from the European Space Agency (ESA) mission *Gaia* (`https://www.cosmos.esa.int/gaia`), processed by the *Gaia* Data Processing and Analysis Consortium (DPAC, `https://www.cosmos.esa.int/web/gaia/dpac/consortium`). Funding for the DPAC has been provided by national institutions, in particular the institutions participating in the *Gaia* Multilateral Agreement. This publication makes use of data products from the Two Micron All Sky Survey, which is a joint project of the University of Massachusetts and the Infrared Processing and Analysis Center/California Institute of Technology, funded by the National Aeronautics and Space Administration and the National Science Foundation.

References

Aringer, B., Kerschbaum, F., & Jörgensen, U. G. 2002, A&A, 395, 915.
Busso, G., Cacciari, C., Carrasco, J. M., De Angeli, F., Evans, D. W., *et al.* 2018, *Gaia DR2 documentation Chapter 5: Photometry*. Tech. rep.
Deason, A. J., Belokurov, V., Erkal, D., Koposov, S. E., & Mackey, D. 2017, MNRAS, 467, 2636.
Frogel, J. A., Mould, J., & Blanco, V. M. 1990, ApJ, 352, 96.
Höfner, S. & Olofsson, H. 2018, A&ARv, 26, 1.
Lebzelter, T., Mowlavi, N., Marigo, P., Pastorelli, G., Trabucchi, M., *et al.* 2018, A&A, 616, L13.
Lindegren, L., Hernández, J., Bombrun, A., Klioner, S., Bastian, U., *et al.* 2018, A&A, 616, A2.
Marigo, P. & Girardi, L. 2007, A&A, 469, 239.
McDonald, I., De Beck, E., Zijlstra, A. A., & Lagadec, E. 2018, MNRAS, 481, 4984.
Mowlavi, N., Lecoeur-Taïbi, I., Lebzelter, T., Rimoldini, L., Lorenz, D., *et al.* 2018, A&A, 618, A58.
Soszyński, I., Udalski, A., Szymański, M. K., Kubiak, M., Pietrzyński, G., *et al.* 2011, AcA, 61, 217.